Effect of Plasma Spray Operating Conditions on Plasma Jet Characteristics and Coating Properties

S. Malmberg and J. Heberlein

Using statistical design of experiments, the arc current, total gas flow rate, percent secondary gas (He), and powder feed rate have been varied to assess the torch behavior and establish its correlation to coating properties. The torch response includes arc voltage drop, torch efficiency, and plasma jet geometry. High-speed images of the luminous plasma jet for each operating condition have been acquired with a LaserStrobe™ videocamera, and image analysis has been used to quantify the jet length and jet fluctuations as additional torch responses. Porosity and unmelted particles, which are determined using image analysis of a micrograph of a NiAl coating cross section, were selected as principal coating characteristics. These findings are expected to be useful for optimization of new spray processes and for evaluation of new torch designs.

1. Introduction

THE properties and quality of a plasma-sprayed coating depend on the operating conditions of the plasma spray system, the size of the plasma jet hot zone, and the heat and momentum transfer from the plasma jet to the particles. The complex nature of a thermal plasma makes theoretical understanding of particle motion and heat and mass transfer difficult.[1] Plasma jet structure and turbulence affect the quantity of air entrainment and, therefore, the heat transfer rates to particles traveling through the plasma jet.[2] Techniques to measure particle size, velocity, and temperature during spraying have been introduced by Fincke et al.[3] and by Vardelle et al.[4] The complexity of these techniques requires long experimental operating times, expensive laboratory equipment, and well-controlled conditions, thereby making extensive experimentation difficult and prohibiting its use in a manufacturing environment. A new technique used here[5] uses the LaserStrobe™ Vision system and image analysis to measure the luminous plasma jet geometry and particle velocity during plasma spraying.

Traditional manufacturing systems control the plasma torch operating conditions based on previous experience in establishing a quality coating, without a fundamental understanding of what occurs in the plasma jet. Previous research[6] has indicated that slight changes in operating conditions greatly affect coating properties. A number of papers, for example Ref 7 to 9, have been dedicated to the use of design of experiments for relating coating properties to the operating parameters used during plasma spraying. Design of experiment techniques have been used to study the effects of operating conditions on the plasma jet and particle velocities as well as the coating properties during plasma spraying.

Key Words: image analysis, microstructure, plasma jet characteristics, spray distribution, visualization

---

S. Malmberg and J. Heberlein, Department of Mechanical Engineering and ERC for Plasma-Aided Manufacturing, University of Minnesota, Minneapolis, Minnesota.

2. Experimental Method

2.1 Plasma Spray System

The orientation of the substrate and coating with respect to the plasma torch is depicted in Fig. 1. The substrate, attached to a rotating 30.5-cm diameter disk, is orthogonal to the torch center line and repeatedly travels past the torch, at a desired traverse velocity. In this way, a coating has been built up layer by layer such that the spray distribution could be analyzed. The Miller SG-100 plasma torch in the subsonic configuration (anode 2083-145, cathode 1083A-129, gas injector 2083-130) was used for all of the experiments, with operating parameters set according to Table 1. Powder was injected at the top of the torch normal to the torch center line with a slight forward angle. The 95/5% NiAl alloy powder (Alloys International 1037) used in these experiments was spherical with a size distribution of 50 to 100 μm, a mean size of 85 μm, and a standard deviation of 12 μm. The particles, suspended in an argon carrier gas flowing at 4.5 slm, enter the 8-mm diameter anode nozzle with a velocity of about 7 m/s. Coatings were formed on a grit-blasted mild steel substrate over a 2-min spraying time without the aid of substrate cooling or preheating.

Arc gas was injected at the base of the cathode such that the gas swirls around the cathode and into the anode nozzle. The swirl motion is used to both stabilize the cathode arc attachment while continuously moving the anode arc attachment reducing the arc spot heat load on the anode.

2.2 Design of Experiments

Design of experiment methods allow the determination of effects of operating parameter variation on responses such as specific coating properties.[10] The typical methodology is to select high and low levels of the operating parameters and through a series of experiments determine the effect of these parameters on the response. The response is any measurable characteristic of the system, i.e., porosity, number of unmelted particles in a coating, arc voltage drop, etc.

A $2^{(6-2)}$ fractional factorial experiment[11] was used to estimate the variation in torch performance and coating quality by

changing the operating parameters. The major operating parameters associated with atmospheric plasma spraying were varied according to Table 1, and both torch and coating characteristics were measured. Argon was used as the primary arc gas and the powder carrier gas, while helium was used as the secondary gas and was either 0 or 10% of the total volumetric arc gas flow rate.

2.3 Torch Characteristics

The amount of energy available to heat the spray particles is the plasma gas energy density, φ, and is defined as:

$$\varphi = \frac{\varepsilon I V}{Q} \qquad [1]$$

where ε is the torch efficiency; I is the operating current; V is the arc voltage drop; Q is the total gas flow rate; and φ is the average plasma gas energy density in J/cm^3 arc gas. Additionally, the geometric size of the hot zone and the trajectory of the spray particles influence particle heating. Images of the luminous plasma jet were recorded using the LaserStrobe™ Vision system at a shutter speed of 1 μs. These images were transferred to a personal computer where a customized version of the NIH image analysis program (Image v1.44) was used to estimate the jet geometry. The luminous jet is characterized by steep gradients of light intensity near its radial edges. Using these light intensity gradients as an edge definition, the width and length of the jet was calculated. The average plasma jet geometry was found by analyzing 40 images of the plasma jet at each operating condition.

The average particle velocities and trajectories for each condition were also found with the LaserStrobe™ Vision system and the image analysis system. For particle velocity measurements, the LaserStrobe™ vision system was used in conjunction with two 337-nm nitrogen lasers. The 3-ns pulsed laser beams exited fiber optic cables with a divergence angle of approximately 20° and illuminated the plasma spray particles. A laser was pulsed during a 50 ns shutter opening, and after a selected time delay, typically 10 μs, the shutter is reopened and the other laser was pulsed. In this way, double exposed images of the particles within the plasma plume were recorded on one frame of the video film. The spatial difference between the particles is divided by the laser pulse time interval and represents the average particle velocity in the image plane. Average particle trajectories were found by determining the particle density as a function of radius from the torch center line at different positions downstream of the torch exit. A more detailed description of the experimental analysis technique for estimation of the luminous plasma jet geometry and particle velocities can be found in Ref 5.

2.4 Coating Characteristics

Coating cross sections, orthogonal to the traverse velocity direction, were prepared so that variations across the spray distribution could be detected. The coating thickness across the spray
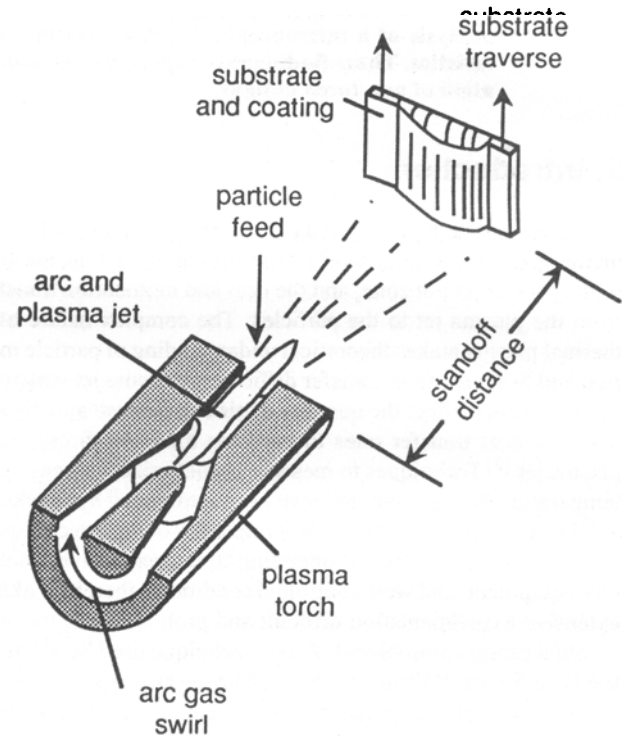

Fig. 1 Schematic of plasma torch and substrate orientation.

Table 1 Experimental Test Matrix

Test No.	Total gas flow rate, slm	Helium, %	Arc current, A	Powder feed, g/min	Traverse velocity, m/s	Standoff distance, cm
1	47	0	700	24.6	0.27	9
2	62	0	700	24.6	0.56	9
3	47	10	700	24.6	0.56	12
4	62	10	700	24.6	0.27	12
5	47	0	900	24.6	0.56	12
6	62	0	900	24.6	0.27	12
7	47	10	900	24.6	0.27	9
8	62	10	900	24.6	0.56	9
9	47	0	700	45.9	0.27	12
10	62	0	700	45.9	0.56	12
11	47	10	700	45.9	0.56	9
12	62	10	700	45.9	0.27	9
13	47	0	900	45.9	0.56	9
14	62	0	900	45.9	0.27	9
15	47	10	900	45.9	0.27	12
16	62	10	900	45.9	0.56	12

distribution (Fig. 2) was measured at 1-mm intervals, with the aid of an optical microscope and an image analysis program. A more detailed explanation of image analysis and its capabilities can be found in Ref 12. The center of the coating, x_c, is found from:

$$x_c = \frac{\int xt(x)dx}{\int t(x)dx} \qquad [2]$$

where $t(x)$ is the coating thickness at the spatial position x on the substrate. The coating width in these experiments is defined as twice the standard deviation, x_{std}, of the thickness distribution and is found from:

$$x_{std} = \left\{ \frac{\int (x - x_c)^2 \, t(x)dx}{\int t(x)dx} \right\}^{1/2} \qquad [3]$$

As described in Ref 13, the coating spray distribution is not necessarily Gaussian and is not centered at the torch axis. Because coating properties such as porosity and unmelt density varied over the spray distribution, average coating property values were calculated from the cross-sectional area within one standard deviation of the calculated thickness center.

3. Experimental Results

3.1 Torch Response

An increase in arc current or a decrease in arc gas flow rate has been found to result in decreased arc voltage. However, these conditions also cause an increase in plasma energy density, which is beneficial to particle heating. The plasma energy density varied from about 11 to 16 J/cm³ and 13 to 21 J/cm³ for the 700- and 900-A current conditions, respectively. In these experiments, torch power efficiency varied from about 50 to 60% and increased with increasing gas flow rate. Consequently, optimizing torch power efficiency is detrimental to the more important parameter of plasma energy density.

Likewise, the luminous plasma jet length has been found to increase with increasing energy density of the plasma gas. The addition of helium had no statistical significance on the plasma jet length. The average luminous jet length varied from about 21 to 30 mm in length for these experiments and had standard de-

viations in length from 2.4 to 4 mm. The average measured jet width at 10 mm from the torch exit ranges from 3.7 to 5.1 mm. On average, jet width increased about 0.56 mm when the current was increased from 700 to 900 A and decreased about 0.43 mm when operating with carrier gas flowing as opposed to no carrier gas. Total arc gas flow and the presence of helium had no significant statistical effect on jet width. A summary of the results is presented in Table 2.

A 2^3 full-factorial experiment was conducted using the argon, helium, and current conditions of Table 1 to find the operating parameter effect on particle trajectories and velocities. The centers of the trajectories for the particles exiting the plasma jet all tend to drop below the geometric center line of the torch. This would indicate that the particles do not receive the maximum benefit of heating and acceleration from the plasma jet. The results (Fig. 3) show the range of the centers of trajectories for the high and low current conditions. The trajectories have not been found to be a function of the operating conditions used in these experiments; however, the range of variation in trajectories indicates a need for better control of the trajectories to obtain repeatable spraying conditions. Indications are that neither powder feed rate nor carrier gas flow rate greatly affect particle trajectory when operating with vortexed arc gas flow.

Increasing the current has the most statistically significant effect on increasing particle velocities. It has been found here and in Ref 3 that the total gas flow rate or addition of helium did not affect particle velocities in a statistically significant way. The range of average particle velocities for the high and low current
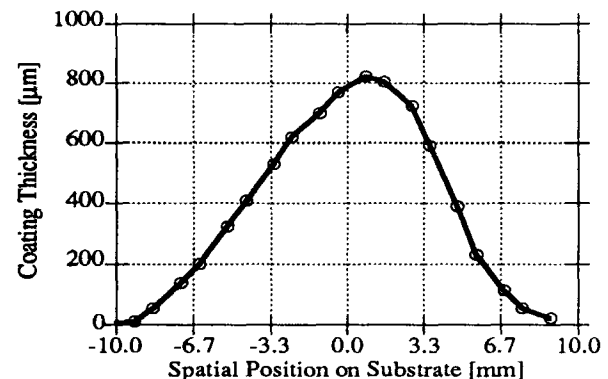

Fig. 2 Typical coating thickness distribution (corresponds to test Condition 11 of Table 1).

Table 2 Summary of Experimental Results

Numeric values indicate the average change in the results when the operating parameter is switched from the low to high condition of Table 1.

Operating parameter	Jet length, mm	Jet width at 10 mm from exit, mm	Deposition efficiency, %	Coating thickness, μm	Coating width, μm	Unmelt density, #/mm²
Average of experiment	24.2	4.44	57.2	578	3.83	14.79
Total gas flow rate	−1.9	—	−3.83	+80	−0.58	+5.69
Helium, %	—	—	+5.43	—	+0.31	−5.06
Arc current	+2.0	+0.56	+6.53	—	+0.62	−4.91
Powder feed rate	NT	NT	+2.98	+375	—	−5.79
Traverse velocity	NT	NT	—	—	—	—
Standoff distance	NT	NT	—	−119	+0.82	—
Carrier gas (off or on)	—	−0.43	NT	NT	NT	NT

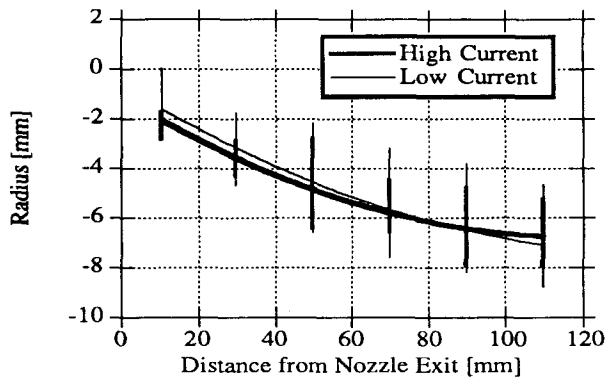Note: — Indicates not statistically significant; NT indicates not experimentally tested.

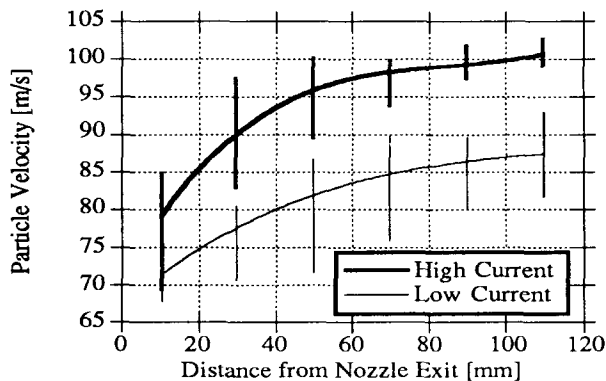**Fig. 3** Particle trajectory for the 700- and 900-A condition.

Fig. 4 Particle velocity for the 700- and 900-A condition.

Fig. 5 Coating deposit efficiency increases with an increase in average plasma energy density and the addition of helium to the arc gas. Arrows indicate decreased gas flow.

conditions (Fig. 4) shows the effect of current. At 110 mm from the torch exit, which is the typical standoff distance for atmospheric plasma spraying, particle velocities are about 87 m/s for the 700-A current condition and about 101 m/s for the 900-A current condition. The axial velocity ranges close to the nozzle exit indicate that a high current causes a higher initial particle acceleration. This has been predicted on the basis that higher currents lead to a lower particle Reynolds number, and as indicated by Ref 14, this leads to a higher coefficient of drag and consequently higher particle acceleration.

3.2 Coating Quality

The average deposition efficiency for the 16-run experiment listed in Table 1 was 57%. As indicated in Fig. 5, the deposition efficiency increased with increasing plasma jet energy density. The addition of 10% helium to the arc gas was statistically significant in increasing the deposition efficiency, and this is attributed to the high thermal conductivity of helium compared to that of pure argon. Surprisingly, an increase in particle feed rate also led to higher deposition efficiencies, which suggests that more of the powder entered the plasma hot core. All of the coatings analyzed were formed over a 2-min spray time using the rotating substrate holder described in Section 2.1.

The spray distribution geometry can be broken into the width, as described above, the maximum coating thickness, and the thickness asymmetry. An increase in energy density of the plasma jet and the addition of helium contributed to an increase in coating width. The average coating width was 7.66 mm. When the current was chan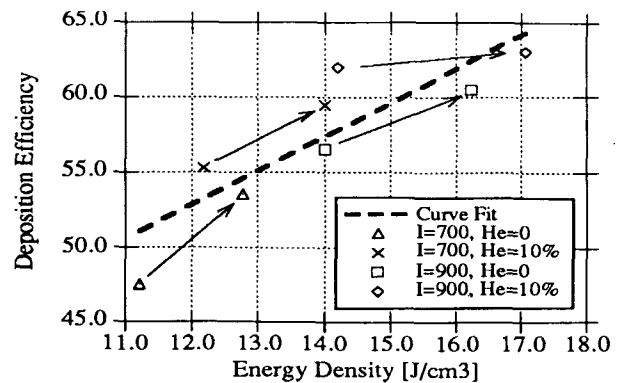ged from 700 to 900 A, the coating width increased about 1.2 mm. Likewise, when decreasing the total gas flow rate from 62 to 47 slm, the coating width increased about 1.2 mm. The coating width increased about 1.6 mm when the standoff distance was changed from 9 to 12 cm, indicating the divergence of the spray pattern. The average coating thickness was 390 and 766 μm for the low- and high-powder feed rate conditions, respectively. As expected, the coating thickness was greatly influenced by the particle feed rate, doubling in these experiments. However, the width was not affected. An increase in the standoff distance decreased the coating height because the spray distribution had the form of a diverging cone.
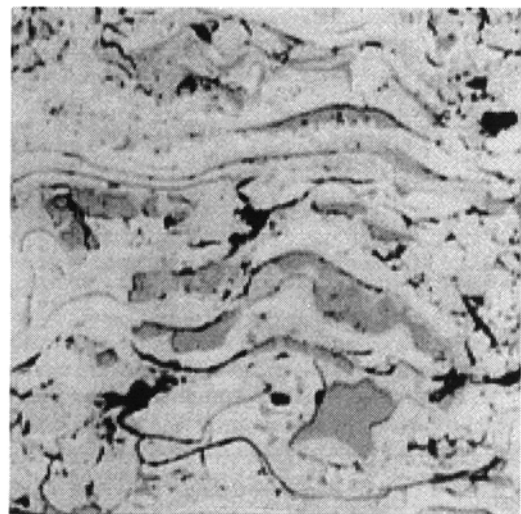
The coating microstructures were analyzed with the aid of an optical microscope and image analysis. For the purpose of consistency, microstructural properties were averaged over measurements taken every millimeter within one standard deviation of the coating center. For example, the coating thickness distribution presented in Fig. 2 had a standard deviation of about 3.5 mm in width, and microstructural properties were averaged from measurements within one standard deviation of the calculated center.

The coating porosity, average pore area (feature area), and the density of unmelted particles were measured. An example of the typical microstructure is shown in Fig. 6, at spatial distances of plus or minus one standard deviation and at the center of the coating distribution. The sum of the dark area regions divided by the area of the coating analyzed is considered an indication of the percentage porosity. Although the true porosity may vary from that measured with image analysis, the relative magnitude of porosity variation from one operating condition to another will quantify the effect of the operating parameters (statistically significant) on porosity. For these experiments, the average porosity of the coatings was less than 1%. An increase in the total arc gas flow rate and standoff distance and the interaction between these two terms were found to be statistically significant in increasing porosity. Likewise, the average feature area of 34 μm^2 was found to increase about 5 μm^2 due to an increase in the total flow rate and the standoff distance. The porosity and feature area were found to be relatively consistent across the coating cross section. Outside of the one standard deviation measurement area, it has been found that porosity increased to above 4%.
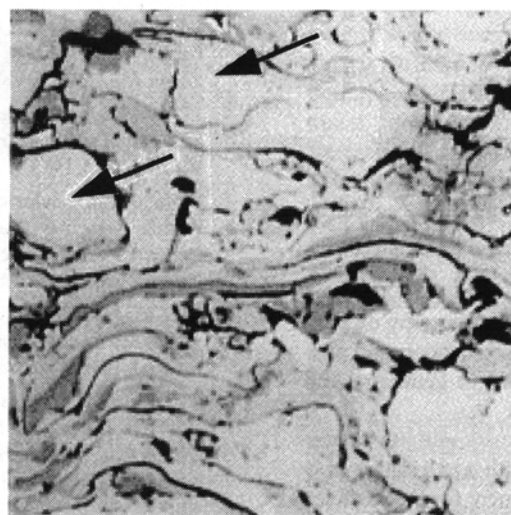
Unmelt density, in this analysis, is defined as the number of unmelted particles per square millimeter. These particles be-
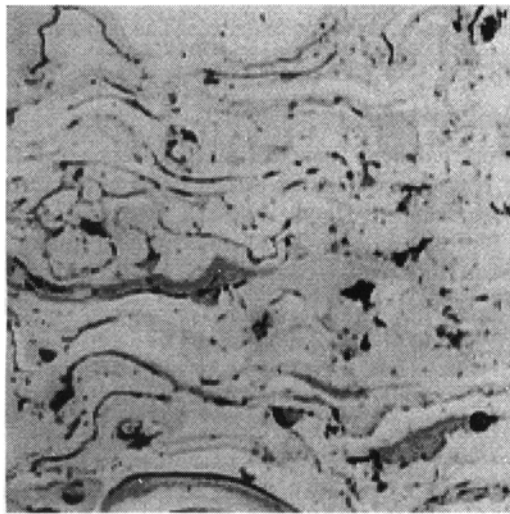
Fig. 6 Typical coating microstructure at (a) –3.5 mm, (b) thickness distribution center, and (c) +3.5 mm. (200 × 200 μm enhanced image).

come trapped within the coating and maintain a resemblance to the original particle geometry (in this case round or near-round shape) and are counted manually. The size of the unmelts in the coating cross section varies; however, an estimate of the average unmelted particle size is not easily obtained because it is not known where the particles are cross sectioned. An example of unmelted particles is indicated by the arrows in Fig. 6(c). For the coatings analyzed in these experiments, it has been found that there was an average of about 15 unmelts per square millimeter. Unmelt density has been found to decrease with an increase in plasma jet energy density, i.e., an increase in current and decrease in total gas flow rate. The addition of 10% helium to the total flow rate has been found to decrease the unmelt density by about 5 mm^{-2}. This decrease in unmelt density is attributed to the high thermal conductivity of helium compared to that of pure argon. In all of the coatings analyzed, both the coating thickness distribution and the unmelt density were located asymmetrically with respect to the coating center. It has been found that the unmelt density is typically five times higher on the steep thickness

gradient side of the thickness distribution with respect to the other side. As shown in Fig. 7, the asymmetry that is present in both the coating thickness distribution and coating unmelt density is due to the direction of vortex arc gas flow. The vortex arc gas flow should be considered together with the position of particle injection, i.e., if the vortex flow is reversed and the powder injection location is changed by 180° about the axis of the plasma effluent, then the same profile is expected. The presence of an asymmetric coating distribution suggests that an enhancement of the particle trajectory is needed to keep the particles in the hot core of the plasma jet.

4. Conclusion

The use of the LaserStrobe™ vision system in conjunction with image analysis has proven to be a quick and useful technique to study the plasma jet and particle flow. By studying the plasma jet, particle velocity, and coating characteristics, a link between the torch parameters and coating quality has been es-
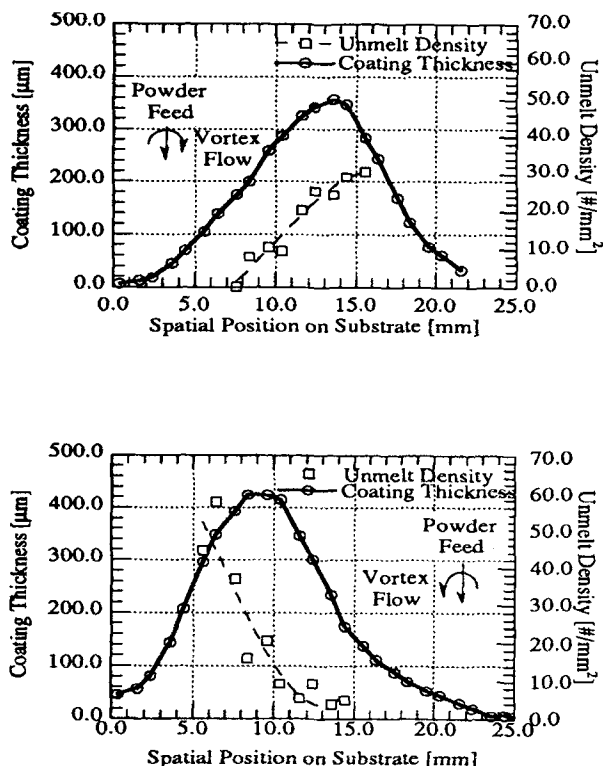
Fig. 7 Examples of coating thickness profiles and unmelt density distributions for clockwise and counterclockwise arc gas vortex direction.

tablished. This diagnostic technique for plasma system characterization is suitable not only for process optimization, but possibly for direct feedback control based on jet geometry and particle flow.

An increase in the plasma jet energy density will provide an increase in the luminous plasma plume width and length that is needed to provide a better heating environment for the particles present in the plasma jet. Increased arc current will increase the particle velocities under typical spray conditions, whereas increasing gas flow rate will not have a significant effect on the particle velocity. Particle velocity has been found to be highest at the axial center line, although the majority of particles fall below the center line. Consequently, to obtain the maximum heat and momentum transfer from the plasma jet to the particles, better control of the spray trajectory is needed, e.g., through more symmetrical powder injection.

An increase in the plasma jet energy density was also found to have the strongest effect in changing coating properties. An increase in the spray deposition efficiency and decrease in the unmelt density have been found with an increase in the arc current and a decrease in the total plasma gas flow rate. A decrease in the total gas flow rate and standoff distance has the most statistically significant effect on decreasing porosity. Porosity measured in these experiments was typically below 1% in the center of the spray distribution, with higher porosity found in the coating edges. The interaction of vortexed arc gas flow and the powder injection location determine the asymmetric coating properties. Although the magnitude of unmelt density can be reduced through an increase in plasma jet energy density, the asymmetry in both the coating thickness distribution and the un-

melt density suggests a need to understand and improve the particle trajectory control.

Acknowledgments

Cited References

1. E. Pfender, Particle Behavior in Thermal Plasmas, *Plasma Chem. Plasma Proc.*, Vol 9 (No. 1), 1989, Suppl, p 167s-194s

2. E. Pfender, W.L.T. Chen, and R. Spores, A New Look at the Thermal and Gas Dynamic Characteristics of a Plasma Jet, *Thermal Spray Research and Applications*, T.F. Bernecki, Ed., ASM International, 1990, p 1-10

3. J. Fincke, W.D. Swank, and C.L. Jeffery, Simultaneous Measurement of Particle Size, Velocity, and Temperature in Thermal Plasmas, *IEEE Trans. Plasma Sci.*, Vol 18 (No. 6), 1990, p 948-957

4. M. Vardelle, A. Vardelle, P. Fauchais, and M.I. Boulos, Plasma-Particle Momentum and Heat Transfer: Modelling and Measurements, *AICHE*, Vol 29 (No. 2), 1983, p 236-243

5. S. Malmberg, J. Heberlein, and E. Pfender, DC Plasma Jet Structure and Particle Velocities During Spraying, *Thermal Spray Conference*, Deutscher Verlag für Schweißtechnik DVS-Verlag GmbH, Düsseldorf, German Welding Society, 1993, p 40-44

6. W.L. Riggs and D. Crawmer, Plasma Spray Booth Equivalency, *Thermal Spray Research and Applications*, T.F. Bernecki, Ed., ASM International, 1990, p 465-484

7. T.J. Steeper, W.L. Riggs, D.J. Varacalle, G.C. Wilson, A.J. Rotolico, and J.E. Nerz, A Design of Experiment Study of Plasma Sprayed Alumina-Titania Coatings, *Thermal Spray: International Advances in Coatings Technology*, C.C. Berndt, Ed., ASM International, 1992, p 415-420

8. R. Kingswell, K.T. Scott, and L.L. Wassell, Optimizing the Vacuum Plasma Spray Deposition of Metal, Ceramic, and Cermet Coatings Using Designed Experiments, *Thermal Spray: International Advances in Coatings Technology*, C.C. Berndt, Ed., ASM International, 1992, p 421-426

9. S.L. Chen, P. Siitonen, and P. Kettunen, Experimental Design and Parameter Optimization for Plasma Spraying of Alumina Coatings, *Thermal Spray: International Advances in Coatings Technology*, C.C. Berndt, Ed., ASM International, 1992, p 51-56

10. S. Bisgaard, Optimizing Thermal Spray Processes Going Beyond Taguchi Methods, *Thermal Spray Research and Applications*, T.F. Bernecki, Ed., ASM International, 1990, p 661-667

11. G. Box, W. Hunter, and J. Hunter, *Statistics for Experimenters*, John Wiley & Sons, 1978

12. J.C. Russ, *Computer-Assisted Microscopy: The Measurement and Analysis of Images*, Plenum Press, 1990

13. B. Champagne and S. Dallaire, Particle Injection in Plasma Spraying, *Thermal Spray: Advances in Coating Technology*, D.L. Houck, Ed., ASM International, 1987, p 25-32

14. E. Pfender and Y.C. Lee, Particle Dynamics and Particle Heat and Mass Transfer in Thermal Plasmas. Part I. The Motion of a Single Particle without Thermal Effects, *Plasma Chem. Plasma Proc.*, Vol 5 (No. 3), 1985, p 211-237